

## Nucleosynthesis in Stars

star: ball of gas in quasi-static equilibrium      gravity  $\leftrightarrow$  pressure

equation of hydrostatic equilibrium

$$\frac{dP}{dr} = - \frac{G m(r) \rho(r)}{r^2} \quad \frac{dm}{dr} = 4\pi r^2 \rho(r)$$
$$\Rightarrow \frac{dP}{dm} = - \frac{G}{4\pi r^4}$$

gravitational collapse of dense molecular clouds

critical Jeans mass

$$M_J \sim \left( \frac{\pi G T}{\mu m_H} \right)^{3/2} s^{-\frac{1}{2}} \sim 1000 M_\odot \left( \frac{T}{10^6 K} \right)^{3/2} \left( \frac{\rho}{10^{-24} g/cm^3} \right)^{-\frac{1}{2}}$$

$\mu$  mean molecular weight

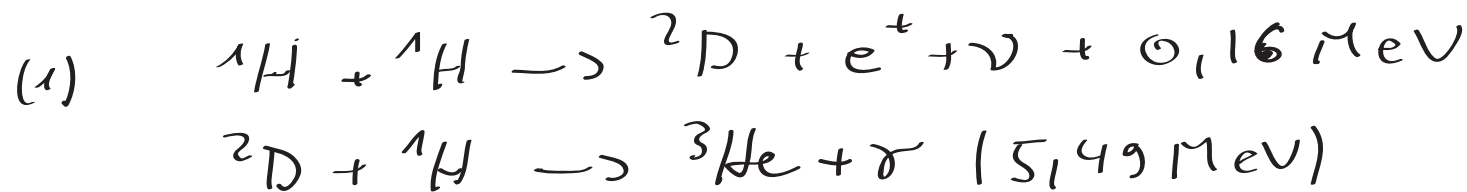
$m_H$  mass of hydrogen atom

## Hydrogen burning

hydrogen burning : 2 processes

- pp chain  
- CNO cycle } effectively  $4p \rightarrow ^4He$

• pp-chain



(1) involves a weak interaction  $\rightarrow$  slow

$$\langle \sigma v \rangle \approx 7,6 \cdot 10^{-44} \text{ cm}^3/\text{s}$$

in center of Sun  $\rho \approx 150 \text{ g/cm}^3$   $X = 0,5$

$$n_p = 6 \cdot 10^{25} \text{ cm}^{-3}$$

$\rightarrow$  hydrogen burning lifetime

$$\tau_{pp} = (n_p \langle \sigma v \rangle)^{-1} \approx 10^{10} \text{ a}$$

remaining reactions are much faster

two branches:

PP-1



PP-2



PP-1 26.20 MeV

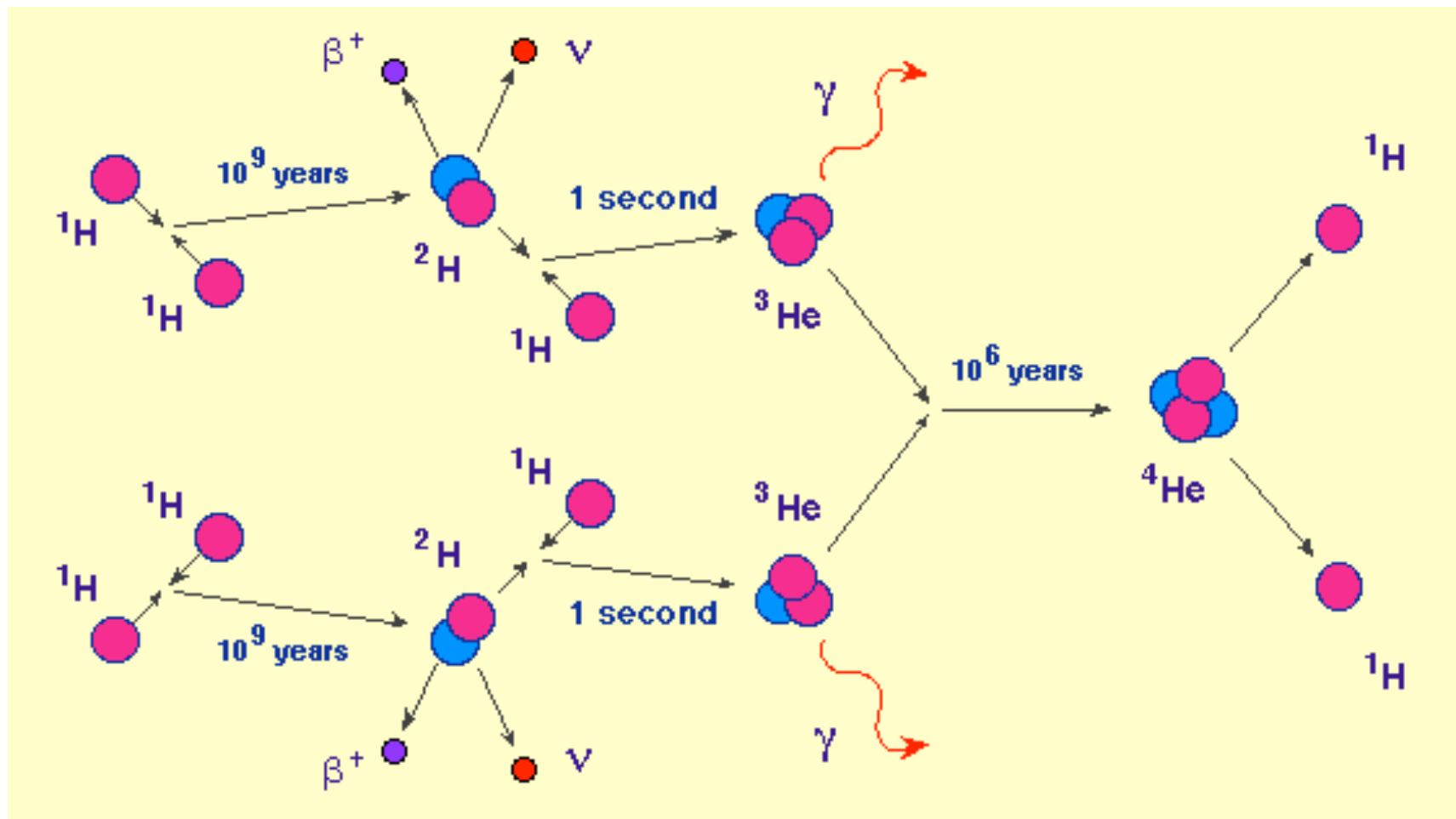
PP-2 25.66 MeV

PP-3 19.17 MeV

Table 5.2. Reactions of the *pp* chains

$p(p, e^+ \nu)d$	$d(p, \gamma)^3\text{He}$	$^3\text{He}(\alpha, \gamma)^7\text{Be}$	$^7\text{Be}(p, \gamma)^8\text{B}$
$^3\text{He}(^3\text{He}, 2p)^4\text{He}$	$^7\text{Be}(e^-, \nu)^7\text{Li}$	$^3\text{He}(\alpha, \gamma)^7\text{Be}$	$^8\text{B}(e^+, \nu)^8\text{Be}^*$
$pp - 1$ (86%)	$pp - 2$ (14%)	$^8\text{Be}^*(\alpha)^4\text{He}$	$pp - 3$ (0.02%)
$Q_{\text{eff}} = 26.20 \text{ MeV}$ (2.0% loss)	$Q_{\text{eff}} = 25.66 \text{ MeV}$ (4.0% loss)		$Q_{\text{eff}} = 19.17 \text{ MeV}$ (28.3% loss)

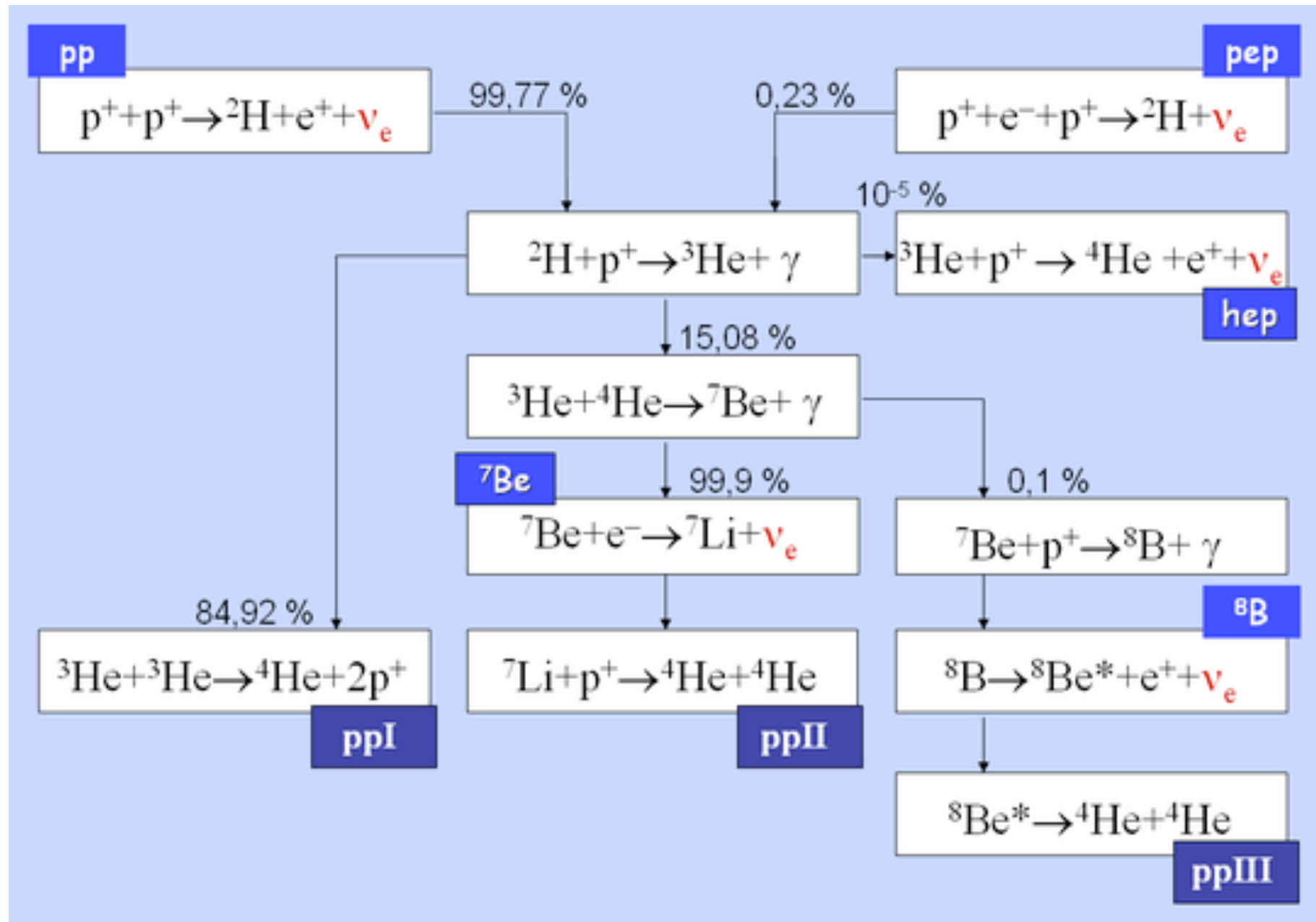
Data from Rolfs and Rodney (1988).

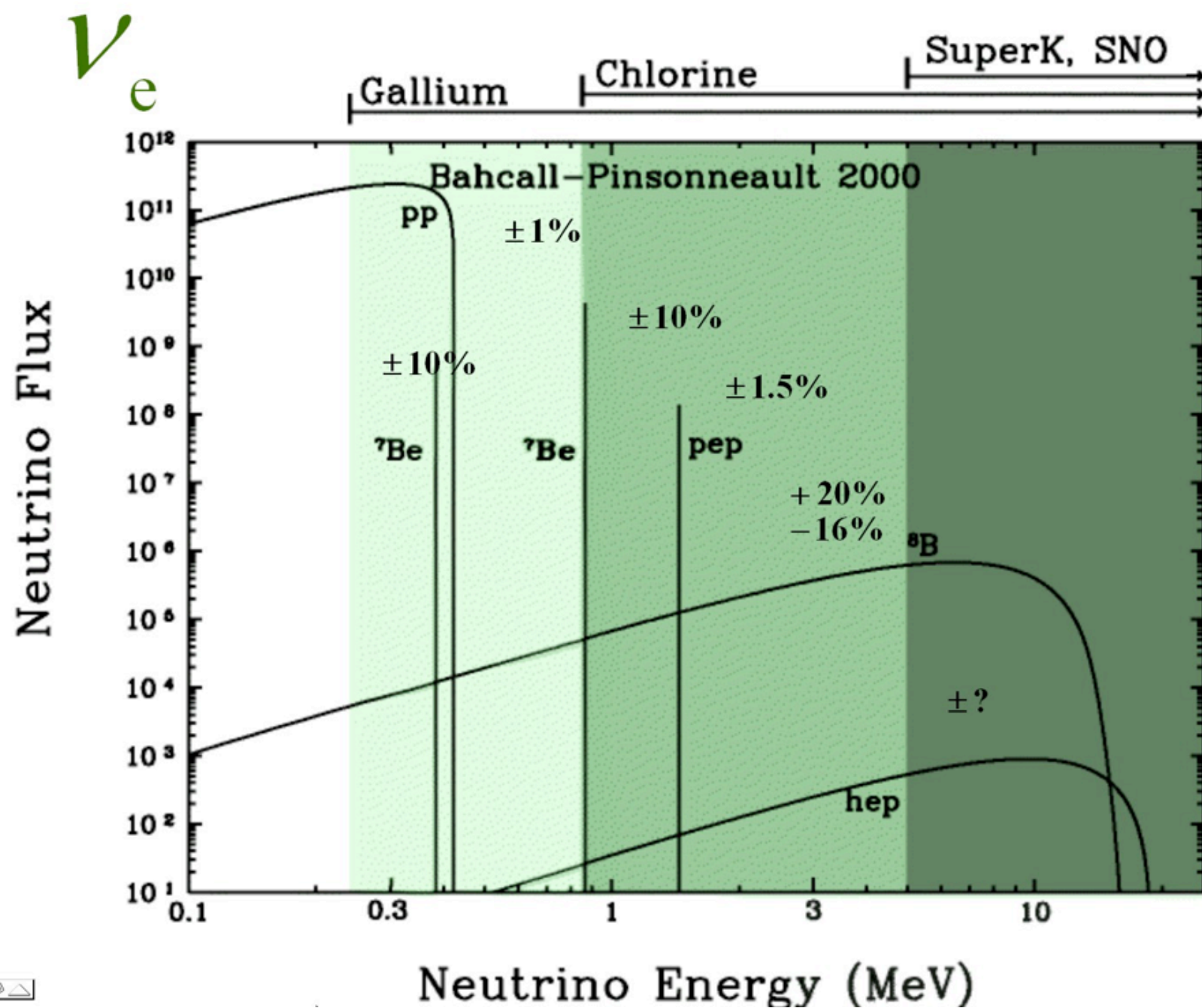


$\nu$  detected in sol  $\rightarrow$  experiments

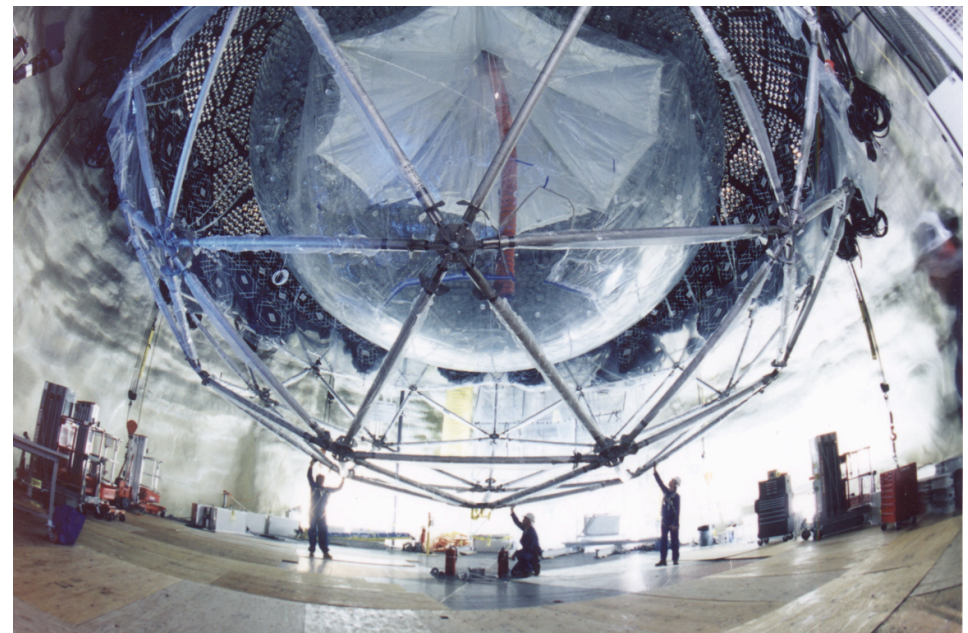
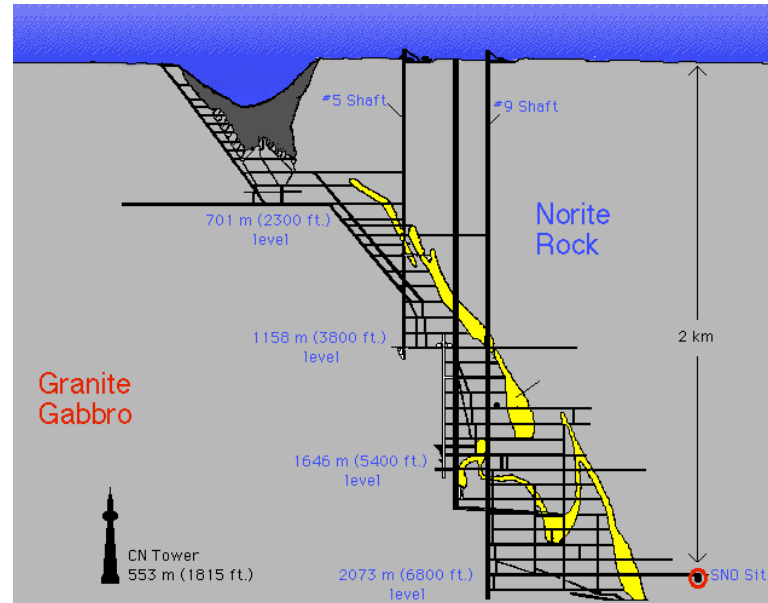
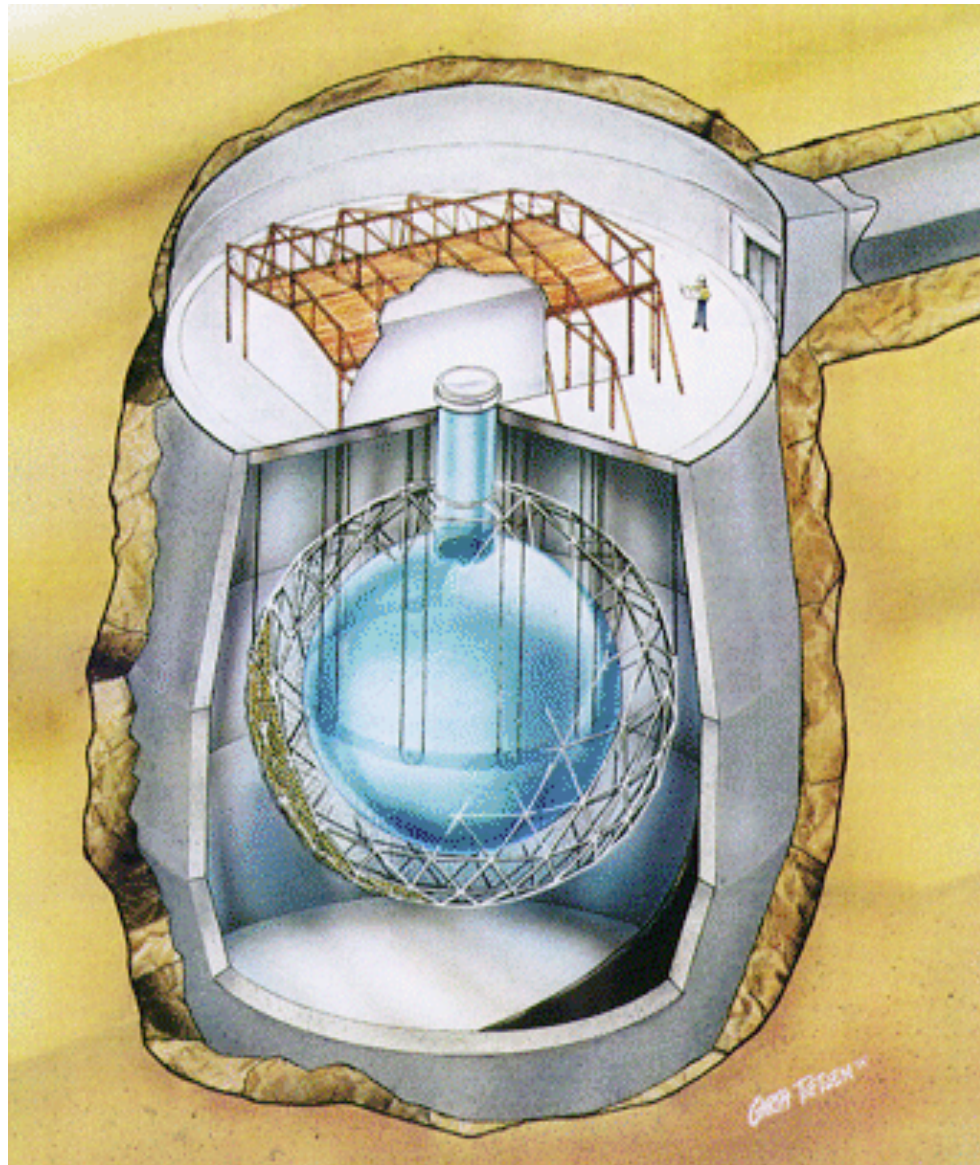
sol-  $\nu$  problem solved by SNO experiment

$\rightarrow \nu$  oscillations



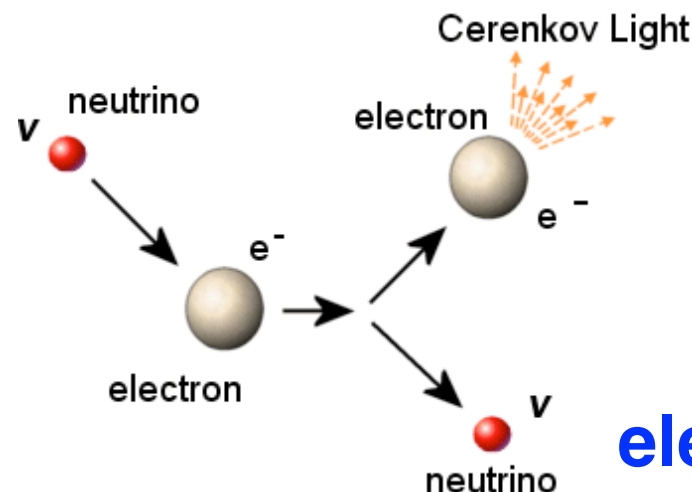
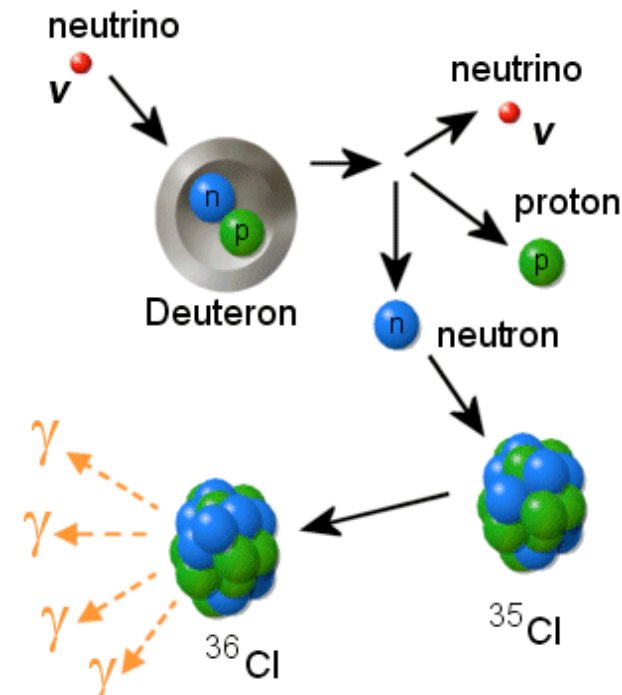
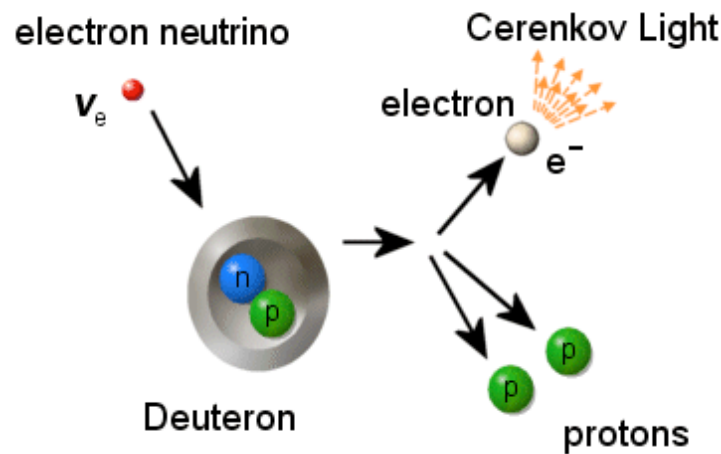


# Sudbury Neutrino Telescope (SNO)



# Sudbury Neutrino Telescope (SNO)

charged-current interaction    neutral-current interaction



electron scattering interaction

Total Rates: Standard Model vs. Experiment  
Bahcall–Pinsonneault 2000

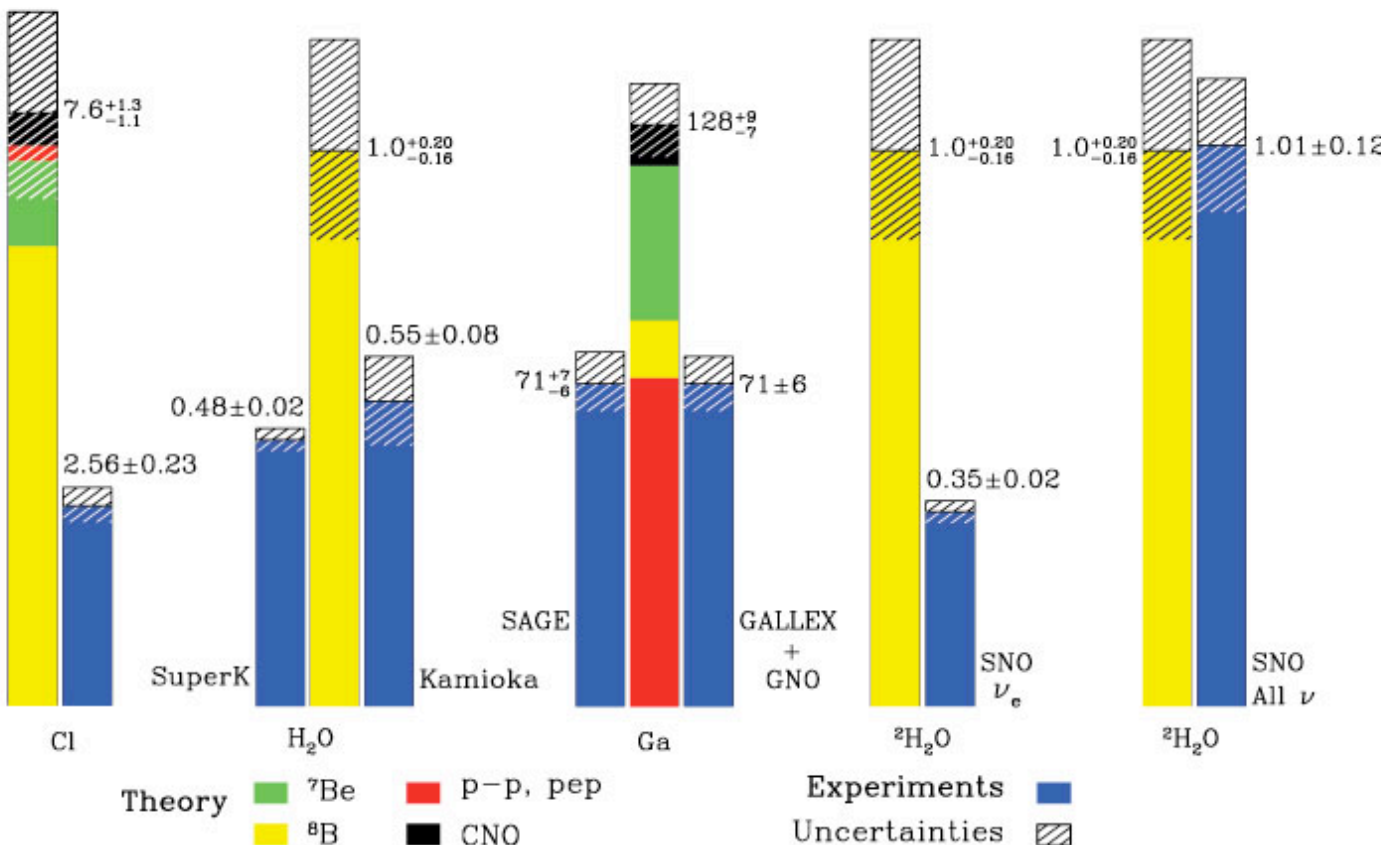


Table 5.3. *Solar neutrino fluxes expected and detected in different experiments*

Detector	Source	Exp. flux <sup>a</sup>	Obs. flux
$^{37}\text{Cl}$	$^7\text{Be}$	1.15	
	$^8\text{B}$	6.20	
	Total	$7.6 \pm 1.2$	$2.56 \pm 0.23$
Kamiokande	$^8\text{B}$	$5.05 \pm 0.9$	$2.8 \pm 0.4$
Gallex, SAGE II	$pp$	70	
	$^7\text{Be}$	34.5	
	$^8\text{B}$	13.1	
	Total	$128 \pm 8$	$75 \pm 8$

<sup>a</sup> For the radiochemical detectors (chlorine and gallium), fluxes are expressed in snu, where 1 snu ('solar neutrino unit')  $\equiv 10^{-36}$  events per target atom per second. For the Kamiokande water detector the unit is  $10^6$  neutrinos  $\text{cm}^{-2} \text{s}^{-1}$ .

After Bahcall, Pinsonneault and Basu (2001).

Table 5.4. *Solar neutrino fluxes from heavy water experiments*

Reaction	Nature	Expected flux <sup>a</sup>	Observed flux
$\nu_e + d \rightarrow p + p + e^-$	Charged current	$5 \pm 1$	$1.76 \pm 0.14$
$\nu_x + d \rightarrow p + n + \nu_x$	Neutral current	$5 \pm 1$	$5.09 \pm 1.0$
$\nu_x + e^- \rightarrow \nu_x + e^-$	Electron scattering	$5 \pm 1$	$2.32 \pm 0.11^b$

<sup>a</sup> In units of  $10^6 \text{ cm}^{-2} \text{s}^{-1}$ , assuming no oscillations.

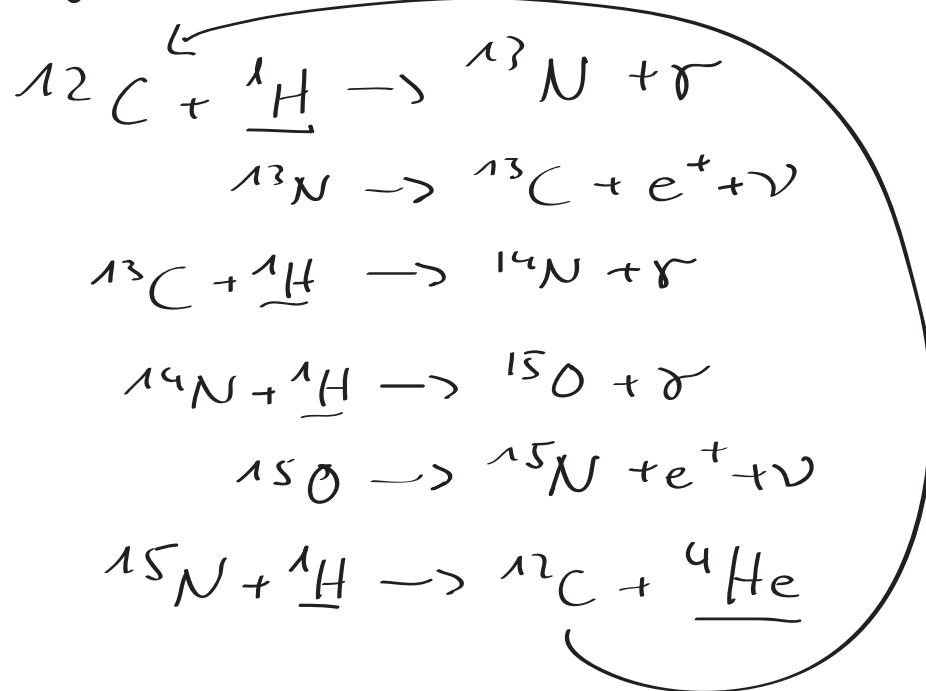
<sup>b</sup> More precise result from Super-Kamiokande.

After Ahmad *et al.* (2002).

- CNO cycle

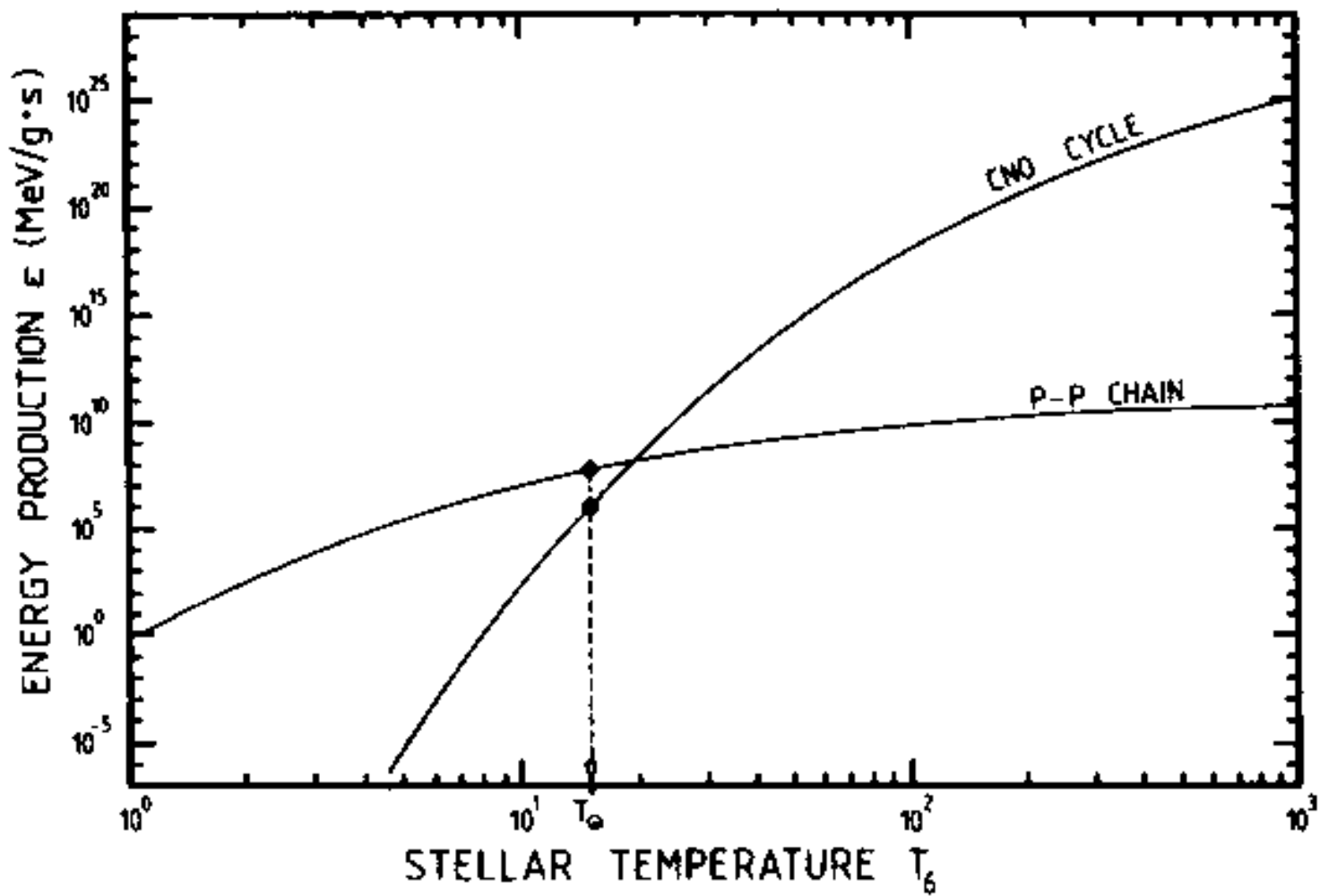
at higher temperatures than inside Sun

hydrogen burning more rapidly by CNO cycle

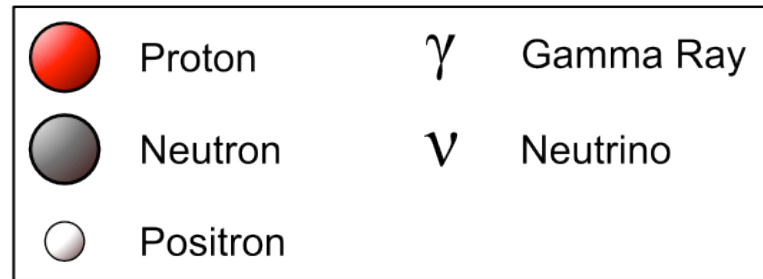
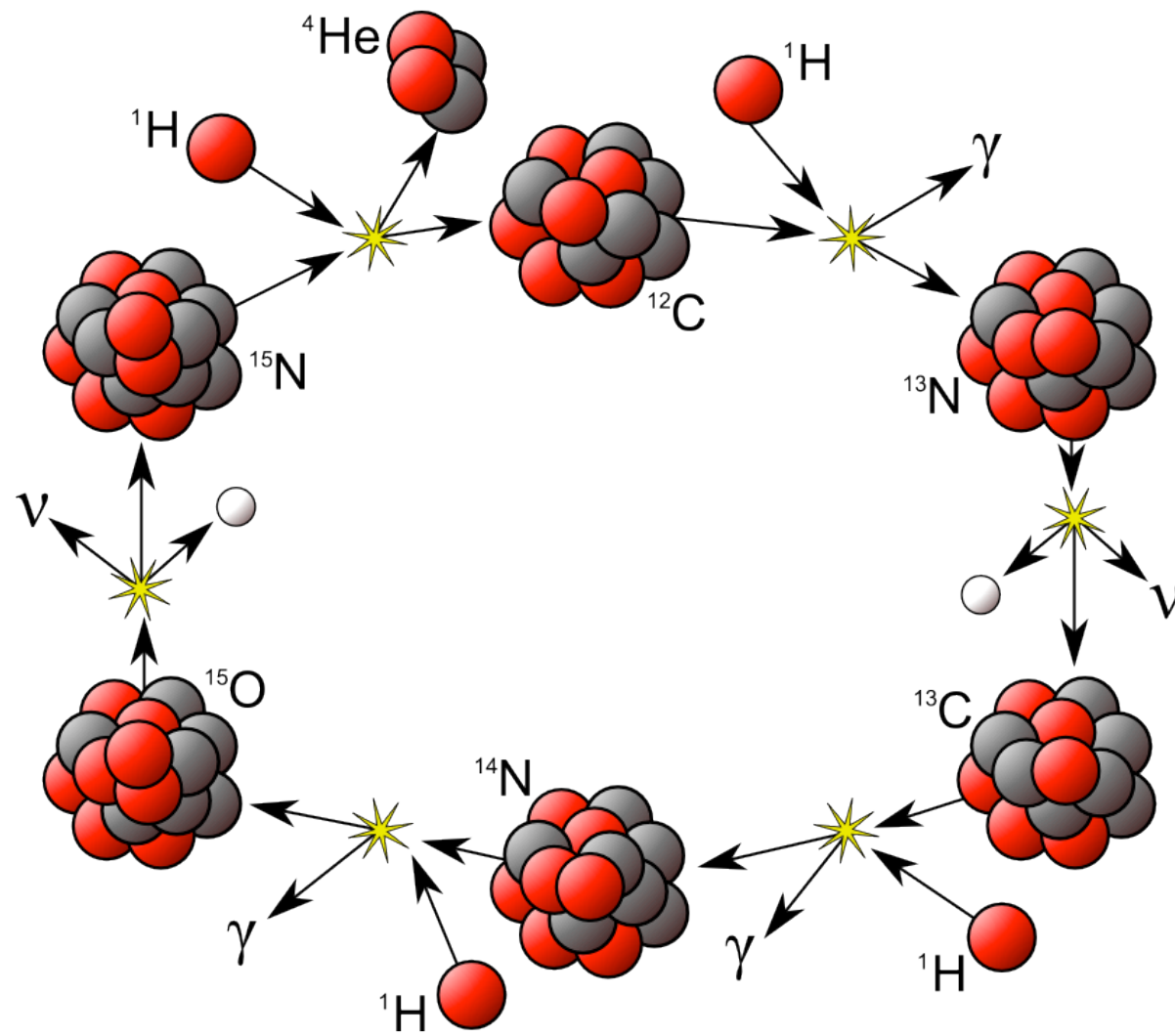


for  $T > 10^7 \text{ K}$ : CNO cycle  $\rightarrow$

Ne-Na cycle  
Mg-Al cycle



**Fig. 5.5.** Dependence on temperature of energy production rates by the *pp* chain and CNO cycle (for solar abundances). After Iben (1965) and Rolfs and Rodney (1988). Copyright by the University of Chicago. Courtesy Claus Rolfs.



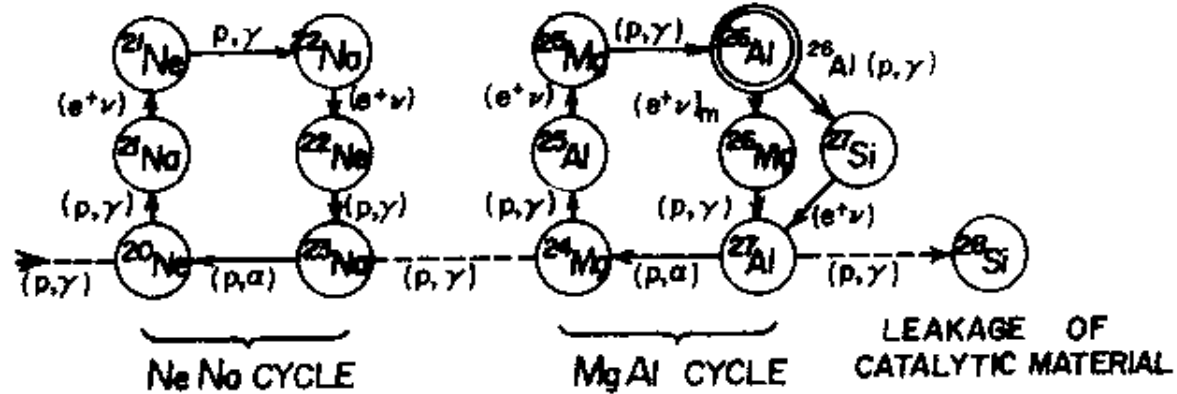
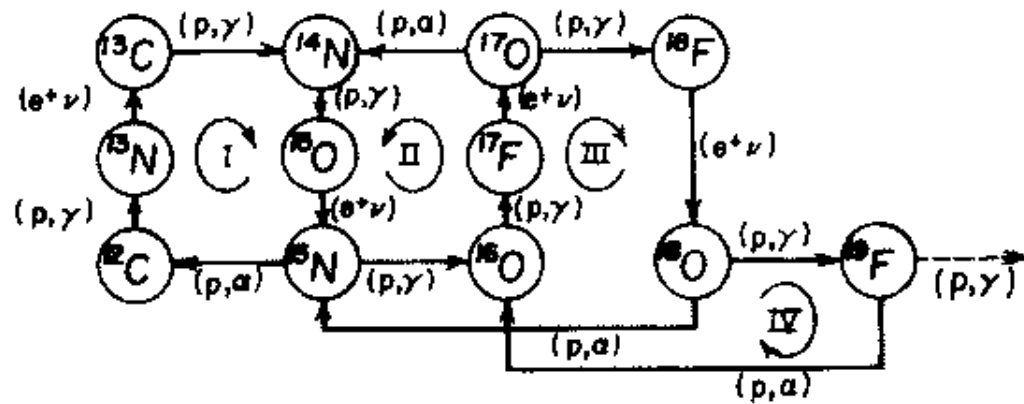


**Fig. 5.6.** CNO tri- and quadri-cycles and Ne-Na and Mg-Al cycles. Adapted from Rolfs and Rodney (1988).

## evolution from the main sequence

when central hydrogen is almost exhausted

- star contracts → heat up interior
- hydrogen is ignited in shell → expansion

after He core reaches amass  $\frac{M_c}{M} \approx 0,09$

core contracts + envelope expands

- red giant

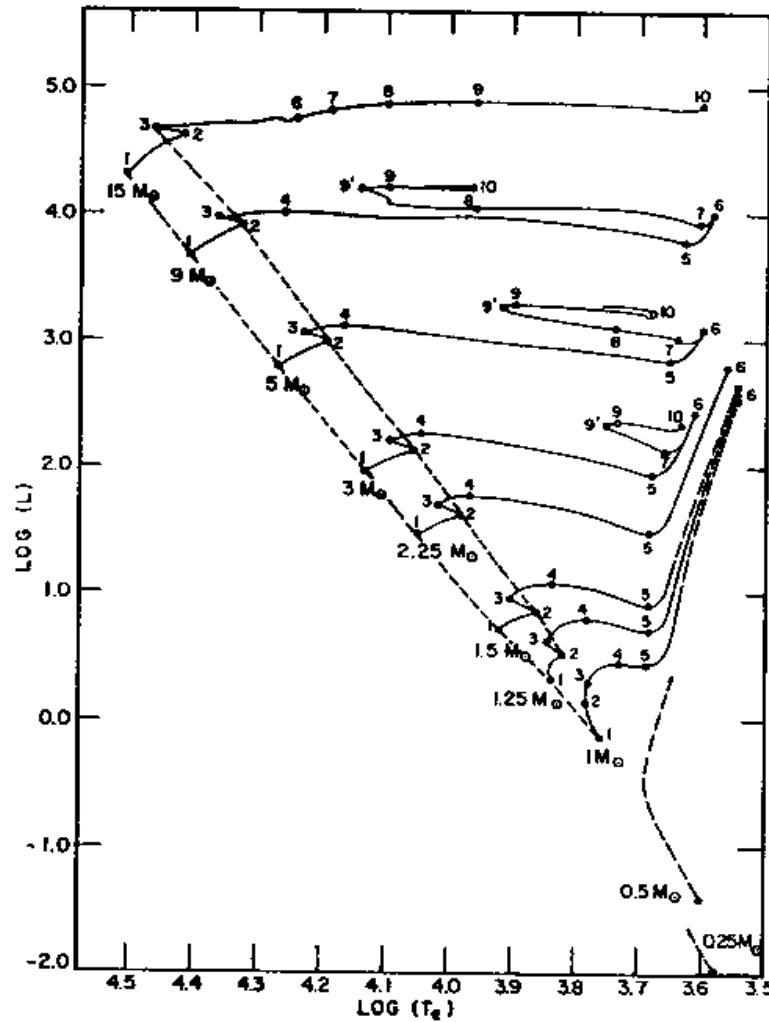
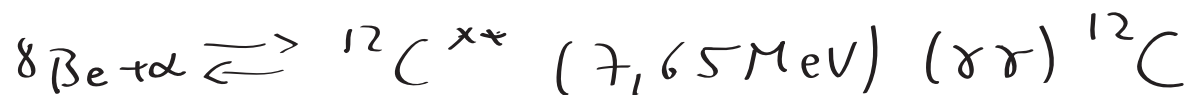


**Fig. 5.7.** Evolutionary tracks for  $Z = 0.02$  (near solar metallicity) stars with different masses in the HR diagram. (Luminosities are in solar units.) Points labelled '1' define the ZAMS and points labelled '2' the terminal main sequence (TAMS), the point where central hydrogen is exhausted. The Schönberg–Chandrasekhar limit may be reached either before or after this (for  $M \geq 1.4 M_{\odot}$ ). Points marked '3' show the onset of shell hydrogen-burning. Few stars are found in the 'Hertzsprung gap' between point '4' and point '5', where the surface convection zone has grown deep enough to bring nuclear processed material to the surface in the first dredge-up. Adapted from Iben (1967).

## Helium burning

at  $T \sim 10^8 \text{ K}$  and  $\rho \sim 10^4 \frac{\text{g}}{\text{cm}^3}$  He burning

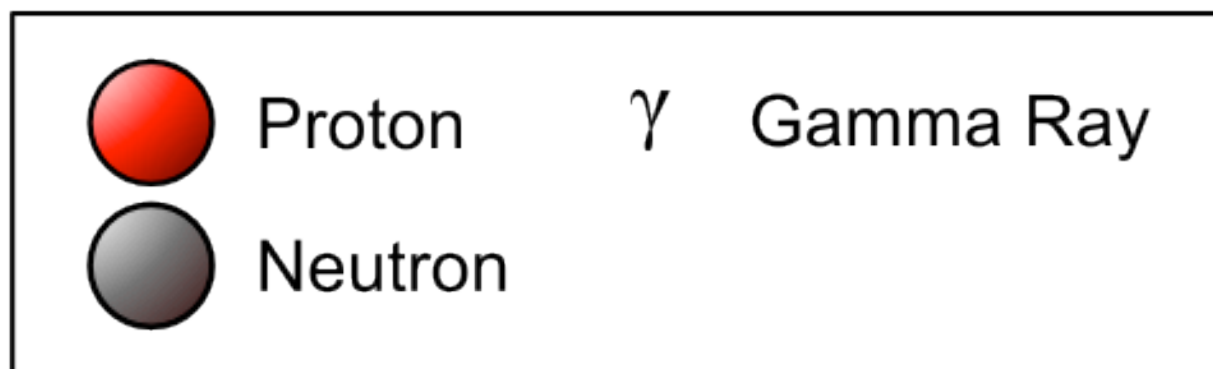
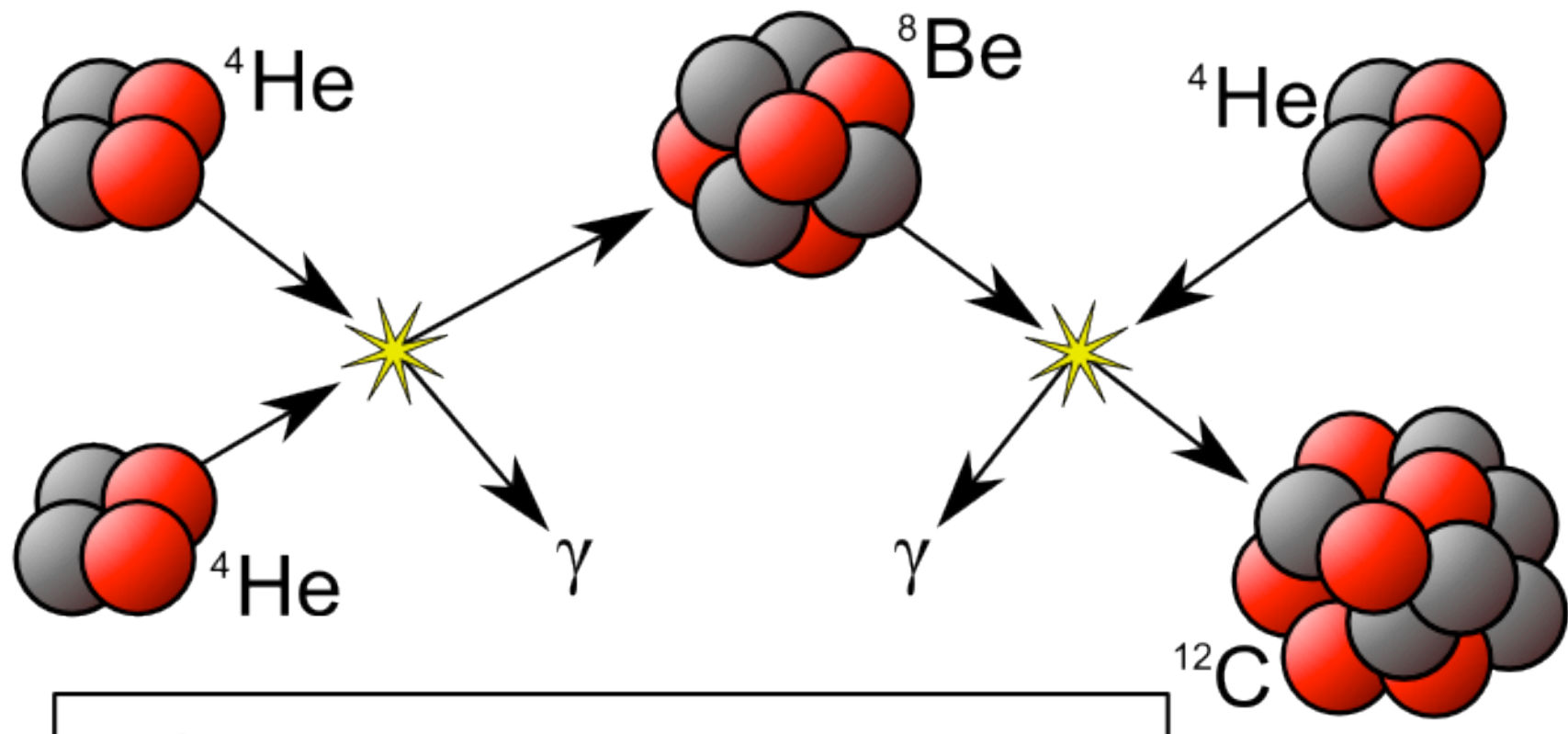
triple  $\alpha$  reaction



nuclear energy levels show remarkable coincidences for creation of elements needed for life:

equilibrium between  $2\alpha$  and  ${}^8\text{Be}$

and  ${}^8\text{Be}$  and excited  ${}^{12}\text{C}$  state



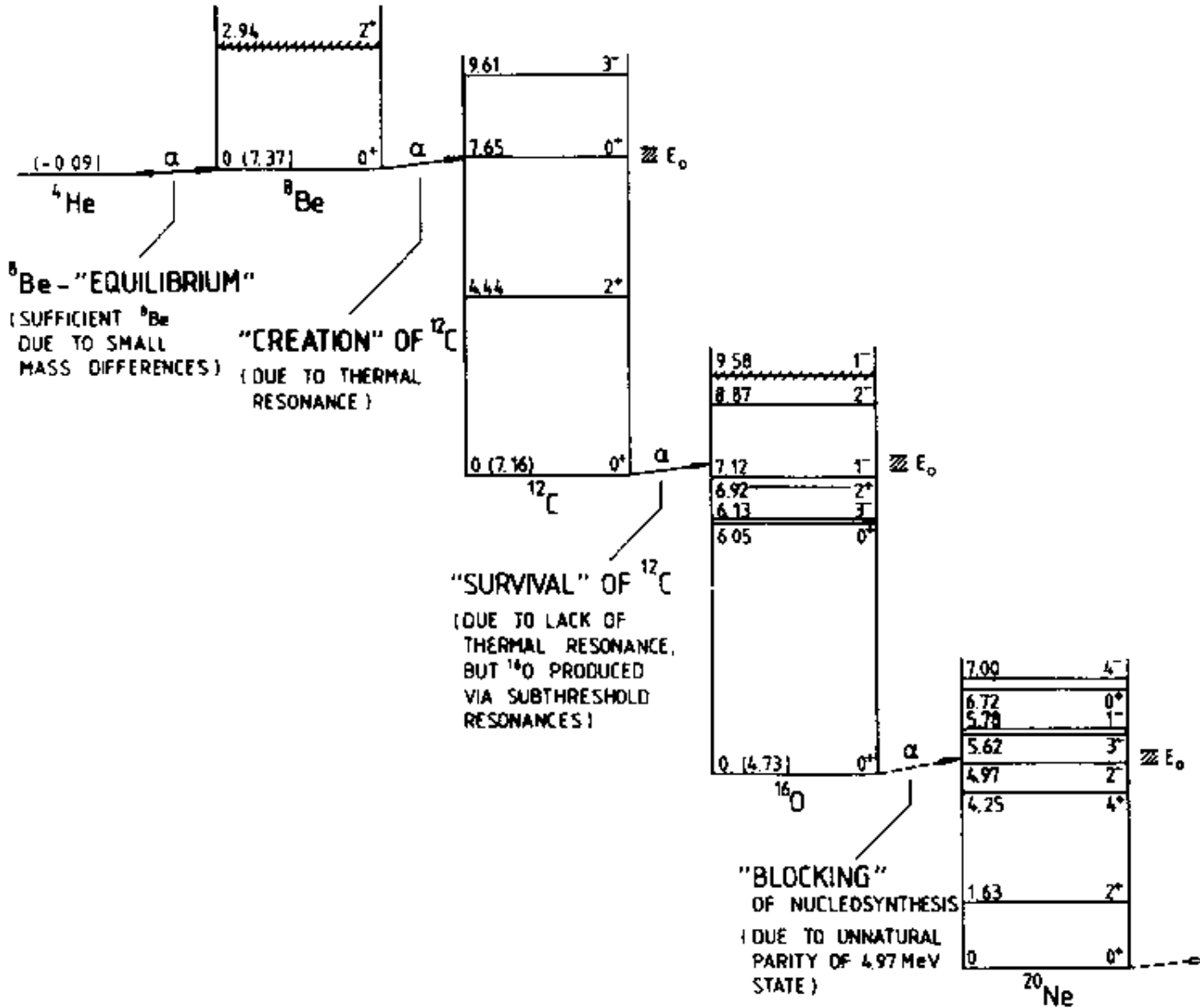


**Fig. 5.8.** Nuclear energy levels involved in the  $3\alpha$  reaction. After Rolfs and Rodney (1988). Copyright by the University of Chicago. Courtesy Claus Rolfs.

important reactions, involving He-burning



He burning on CNO material

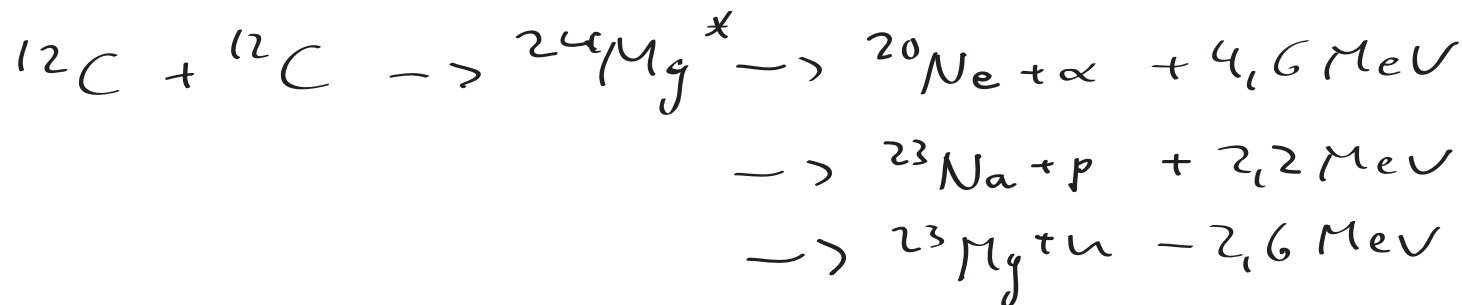


$\rightarrow$  neutron excess

## evolution of massive stars

$M \geq 10M_\odot$ : carbon burning

- C burning  $T \sim 10^9 K$   $t \sim 1000 a$



followed by  ${}^{23}\text{Na}(p, \alpha) {}^{20}\text{Ne}$

- Ne-burning  $T \sim 1.5 \cdot 10^9 K$   $t \sim 1 a$



- O-burning  $T \sim 2 \cdot 10^9 \text{ K}$   $t \sim \frac{1}{2} \text{ a}$



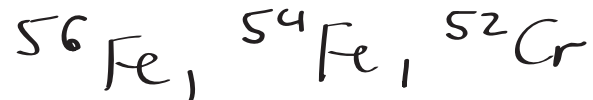
$\Rightarrow$  onion-like structure with increasingly heavy nuclei towards center

- Si-burning  $T \geq 3 \cdot 10^9 \text{ K}$   $t \sim 1 \text{ d}$



followed by  $^{28}Si + \alpha + n + p \rightarrow$  iron peak elements

core is dominated by neutron-rich nuclei:



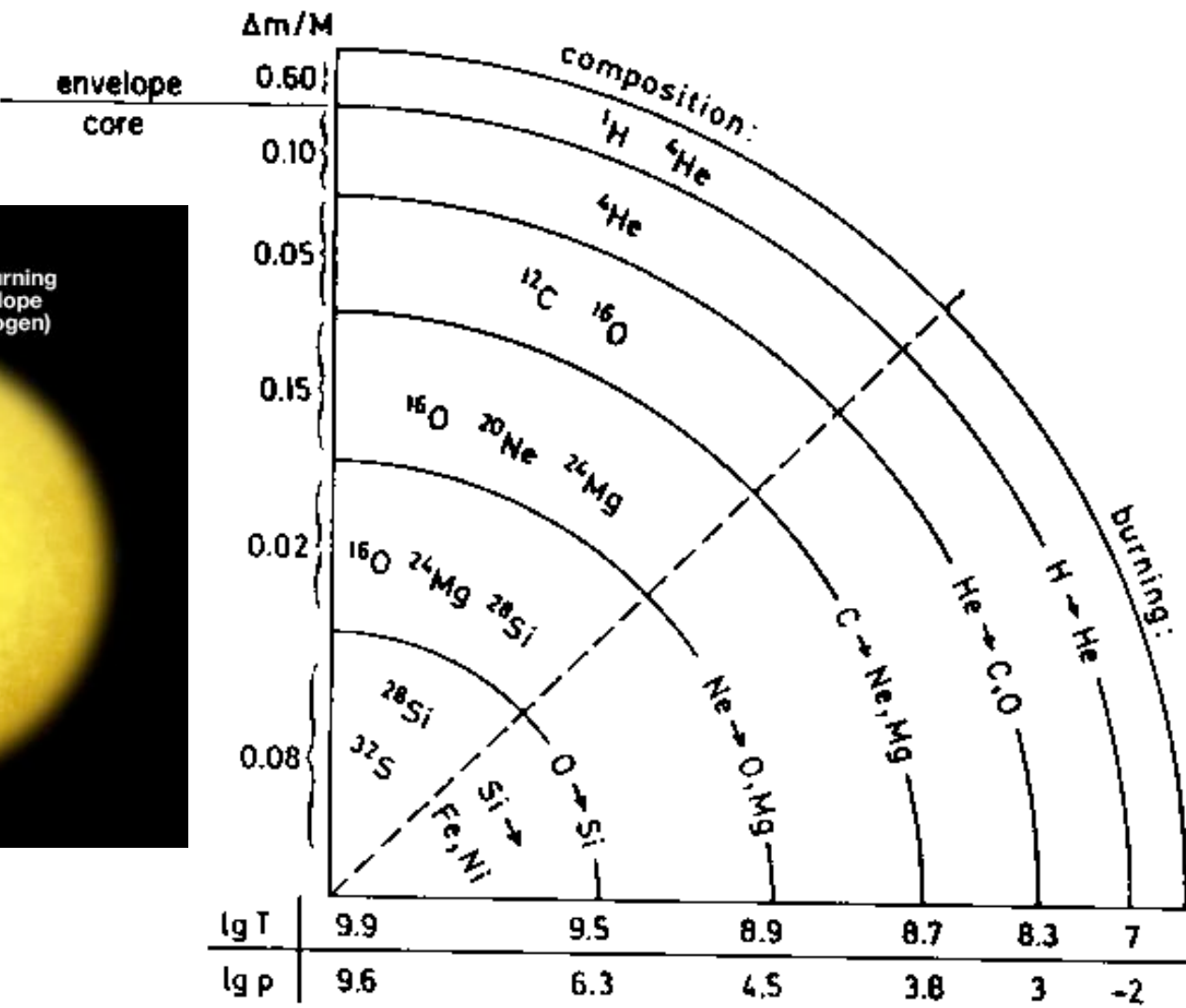
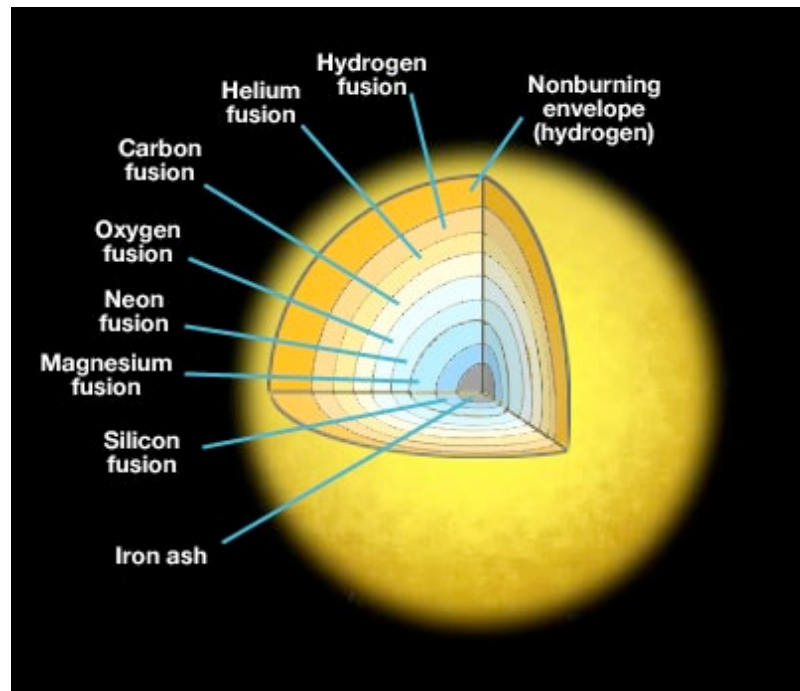


**Fig. 5.9.** Schematic illustration (not to scale) of the ‘onion-skin’ structure in the interior of a highly evolved massive star ( $25 M_{\odot}$ ). Numbers along the vertical axis show some typical values of the mass fraction, while those along the horizontal axis indicate temperatures and densities ( $\text{gm cm}^{-3}$ ). Adapted from Kippenhahn and Weigert (1990).

next stage: dynamical collapse of core  
on ms time scale

caused by electron capture + photo disintegration

disintegration of (Fe) nuclei  $\rightarrow \alpha + p + n$

$e^- + p \rightarrow n$   $\rightarrow$  neutron star

$\rightarrow \gamma$  emission

bounce at nuclear densities

$\rightarrow$  shock propagates outwards

$\rightarrow$  type II supernova

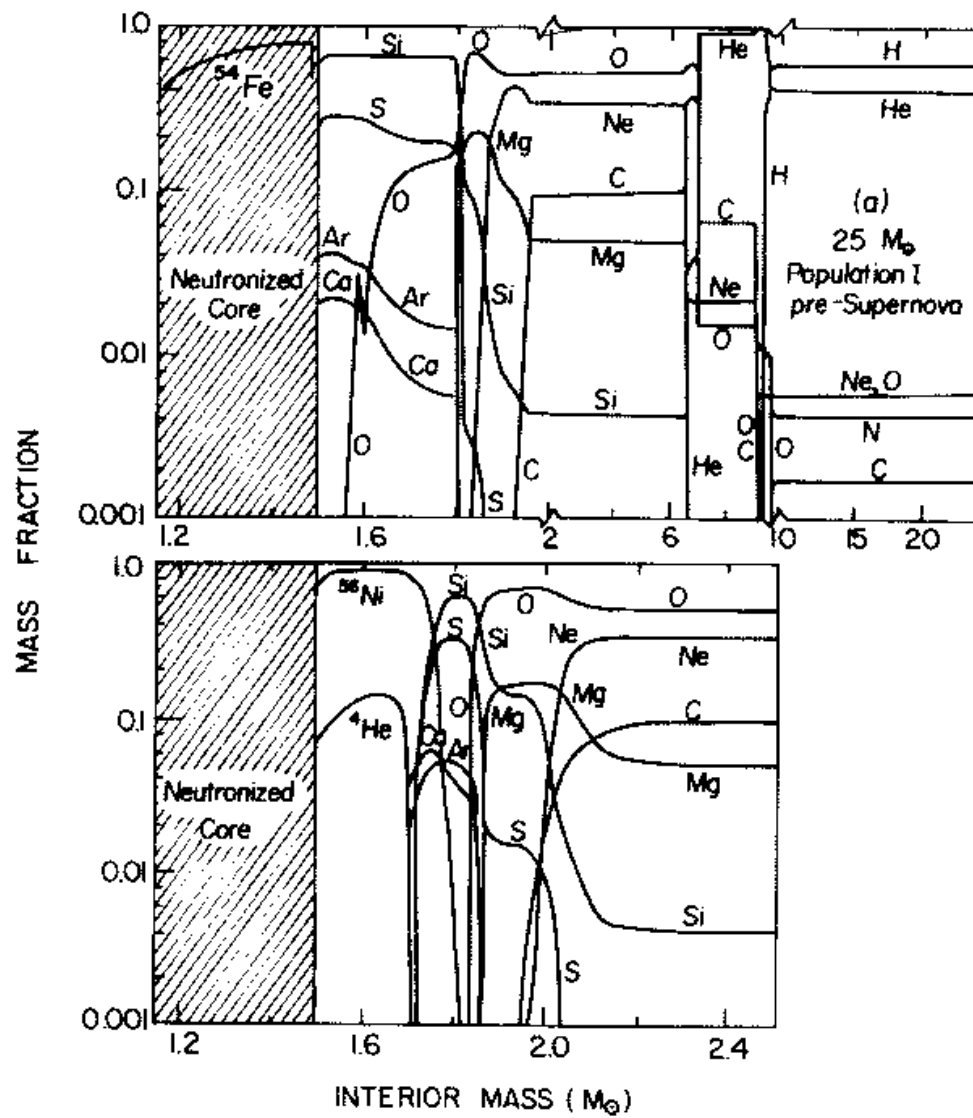


**Fig. 5.10.** Upper panel: chemical profile of a  $25 M_{\odot}$  star immediately before core collapse. (Note change in horizontal scale at  $2 M_{\odot}$ .) Lower panel: the same, after modification by explosive nucleosynthesis in a supernova outburst. The amount of  $^{56}\text{Ni}$  (which later decays to  $^{56}\text{Fe}$ ) ejected depends on the mass cut, somewhere in the  $^{28}\text{Si} \rightarrow ^{56}\text{Ni}$  zone, and is uncertain by a factor of 2 or so. Adapted from Woosley and Weaver (1982).

inner layers modified by explosive synthesis

grav. energy released  $\sim 10^{53}$  erg

99% carried away by  $v$ 's

1% ( $10^{51}$  erg)  $\rightarrow$  shock

$10^{50}$  erg needed to eject the envelope against gravity

$\rightarrow$  elements synthesised in hydrostatic stellar evolution are ejected

explosive synthesis on s timescale

material ejected by SN-II after radioactive decay

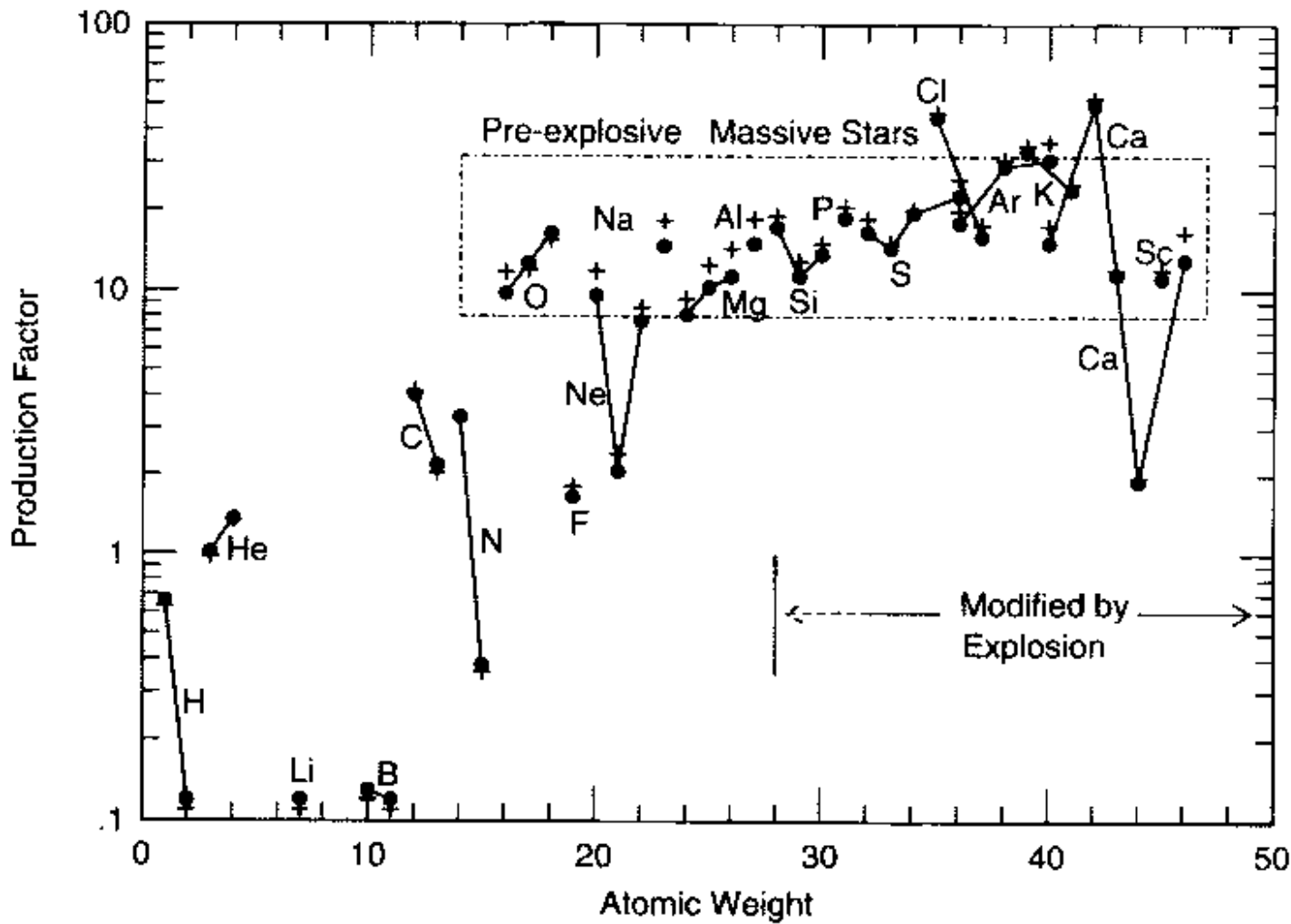


**Fig. 5.11.** Amounts, in units of relative Solar-System abundances, of nuclear species resulting from hydrostatic evolution of an average pre-supernova. Filled circles represent an initial mass function with slope  $-2.3$  and plus signs one with slope  $-1.5$ . The dashed box encloses 28 species co-produced within a factor of 2 of solar values, assuming a  $^{12}\text{C}(\alpha, \gamma)^{16}\text{O}$  rate  $1.7 \times$  that given by Caughlan and Fowler (1988). Reprinted from Weaver and Woosley (1993). Reproduced with kind permission of Elsevier Science. Courtesy Tom Weaver.

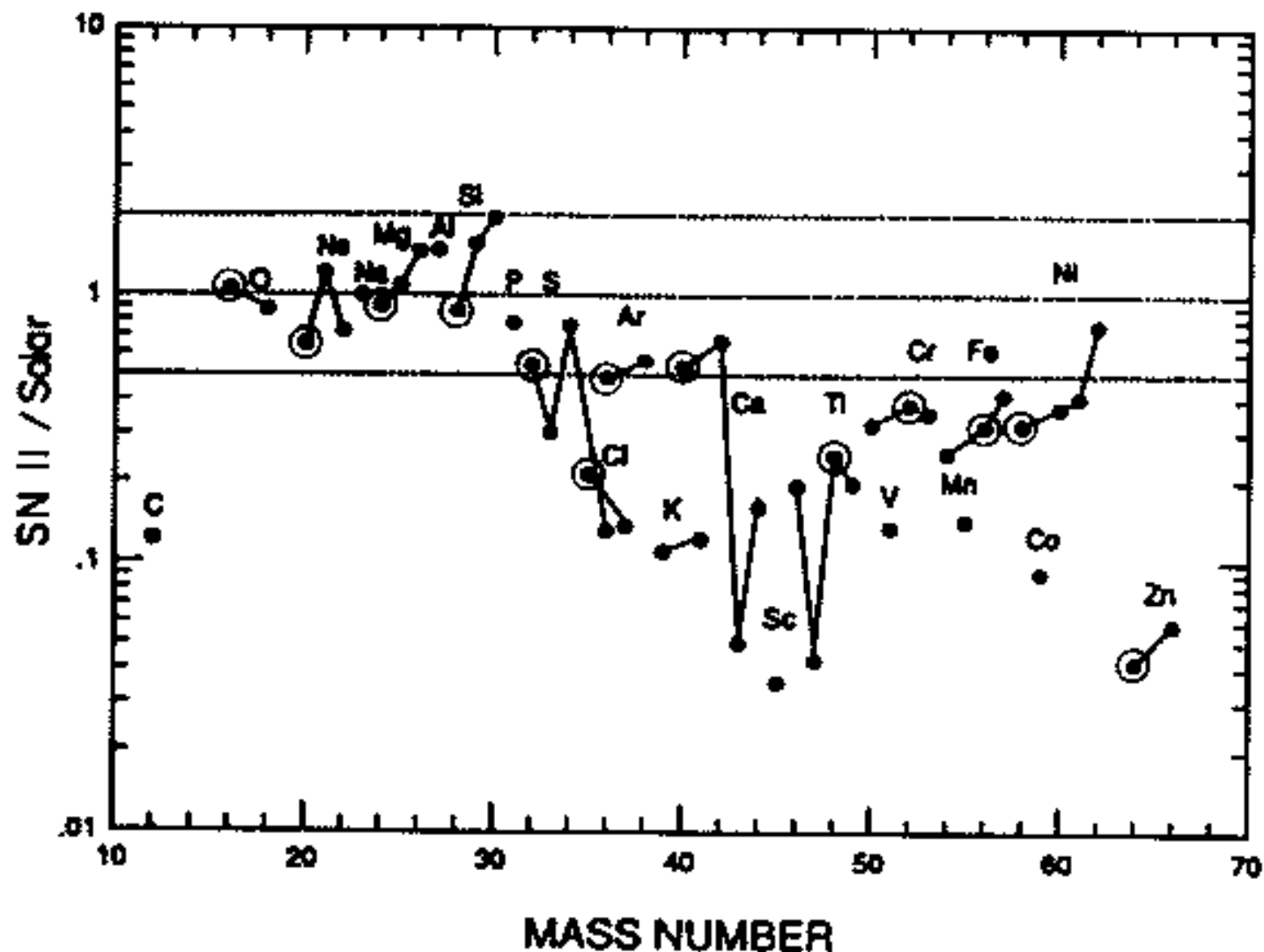


**Fig. 5.12.** Calculated abundances after decay of  $^{56}\text{Ni}$  and other radioactive nuclei, relative to solar, in material ejected from a typical Type II supernova explosion, averaged over initial masses  $10$  to  $50 M_{\odot}$ . Dominant isotopes of each element are circled. Adapted from Tsujimoto (1993).

## evolution of intermediate and low-mass stars

$M \sim 2.5$  to  $8 M_\odot$

CO core not massive enough to ignite C  
→ white dwarf

evolution for  $5 M_\odot$

A hydrogen burning

B H exhausted

C H shell burning

D Hertzsprung gap

E core He burning

F core contracts, envelope expands  
→ white dwarf

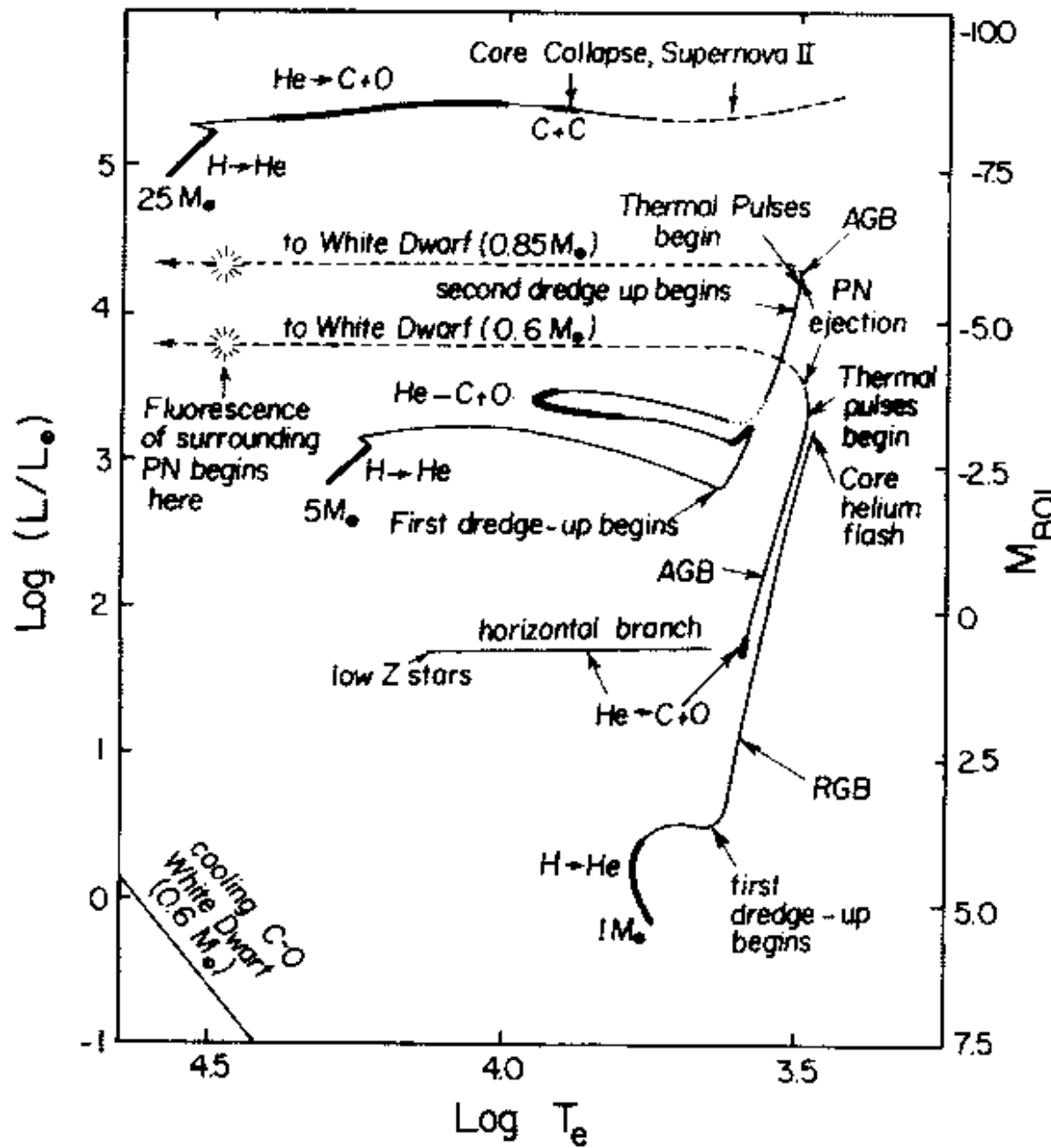


**Fig. 5.15.** Evolutionary tracks of stars with mass 1, 5 and  $25 M_{\odot}$  in the HR diagram. Adapted from Iben (1985, 1991).

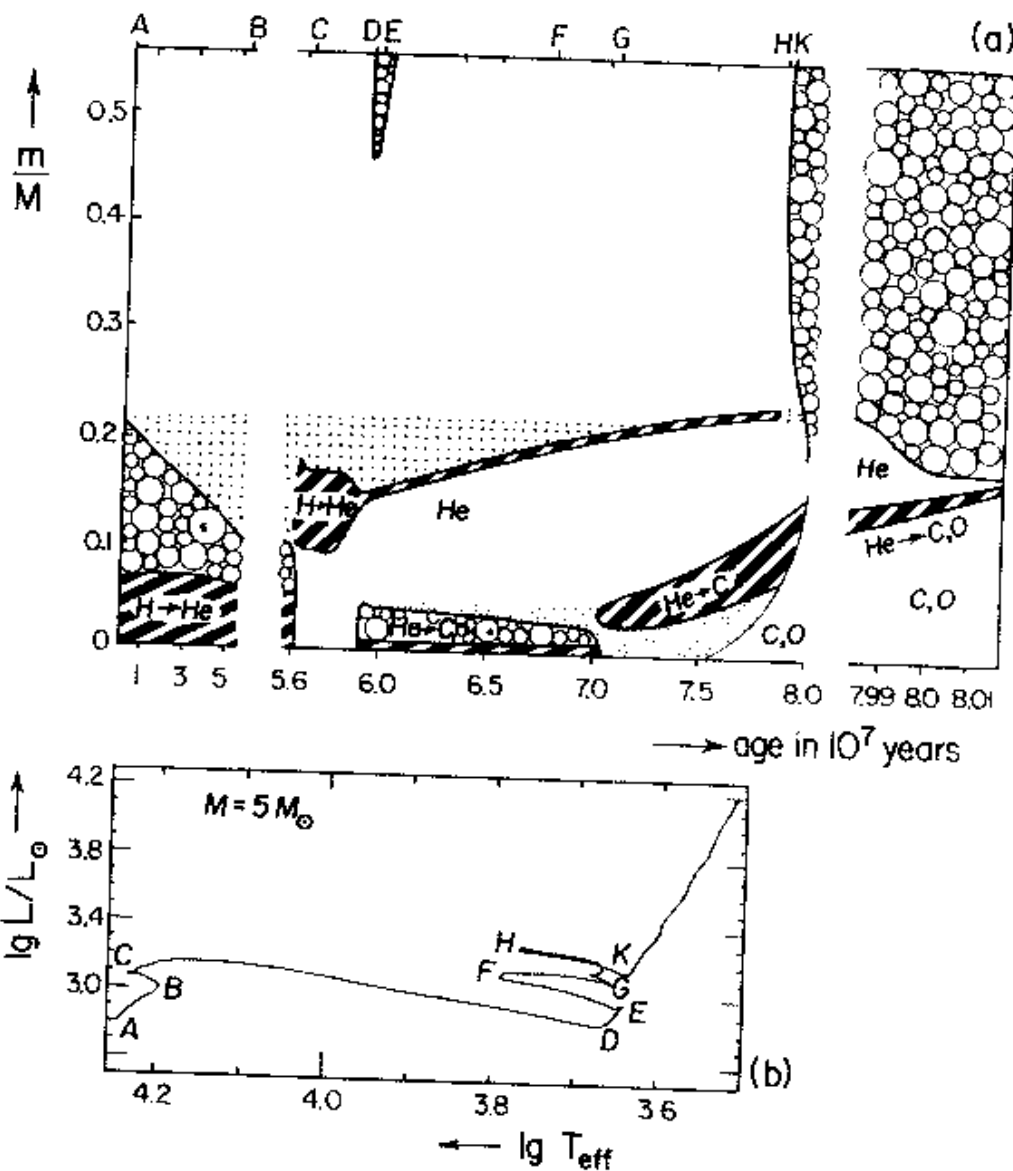


**Fig. 5.16.** Evolution of a  $5 M_{\odot}$  star of extreme Population I, shown in chemical profile and in the HR diagram. ‘Cloudy’ areas indicate convective regions; heavily hatched areas indicate significant nuclear energy generation ( $> 10^3 \text{ erg gm}^{-1} \text{ s}^{-1}$ ); and dotted areas are regions of variable chemical composition. After Kippenhahn and Weigert (1990). Copyright by Springer-Verlag.

## interacting binary stars

accretion of mass from one star to other

mass transfer red giant  $\rightarrow$  white dwarf

unburned H piles up on WD

envelope  $\sim 10^{-5} - 10^{-4} M_\odot$

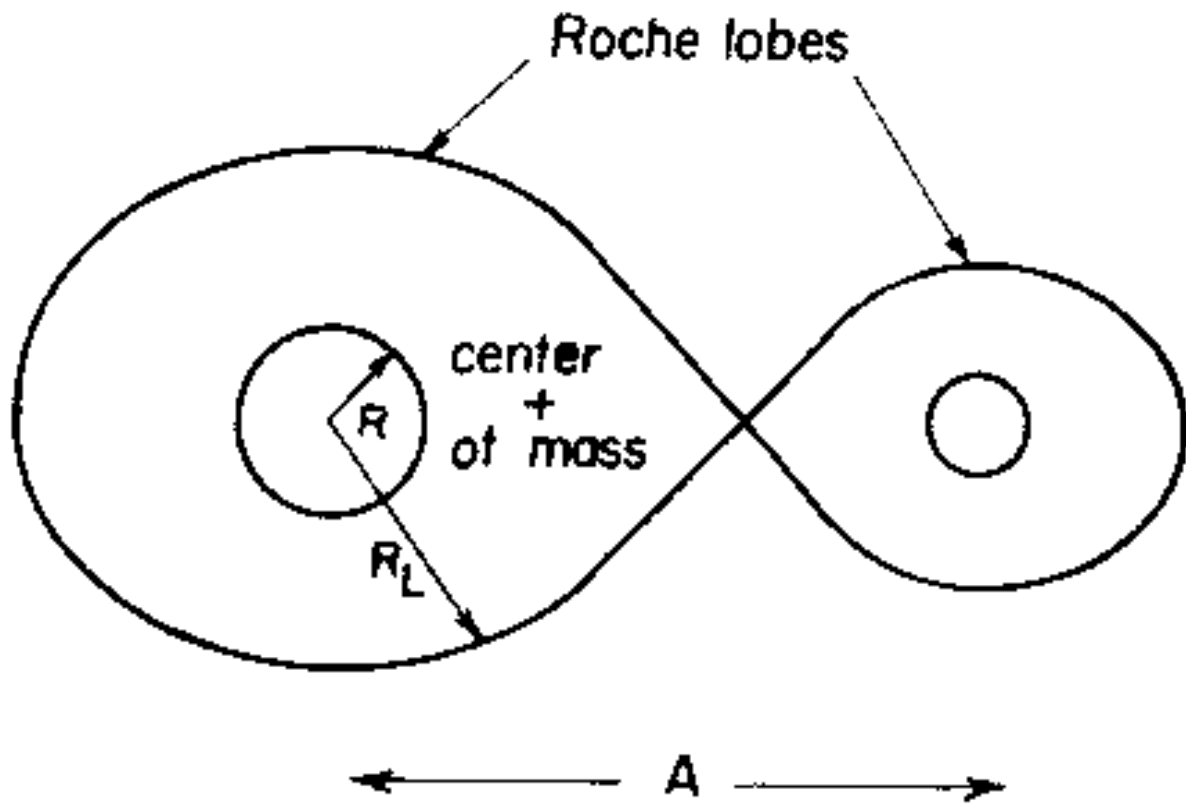
ignition of fast CNO cycle

$\rightarrow$  thermonuclear runaway

SNIa: accretion of material on WD

$\rightarrow$  Chandrasekhar mass  $1.4 M_\odot$

$\rightarrow$  explosive C burning



$$R_{iL} \sim 0.52 \left( \frac{m_i}{m_{\text{tot}}} \right)^{0.44} A$$

**Fig. 5.22.** Roche-lobe geometry. Adapted from Iben (1991).

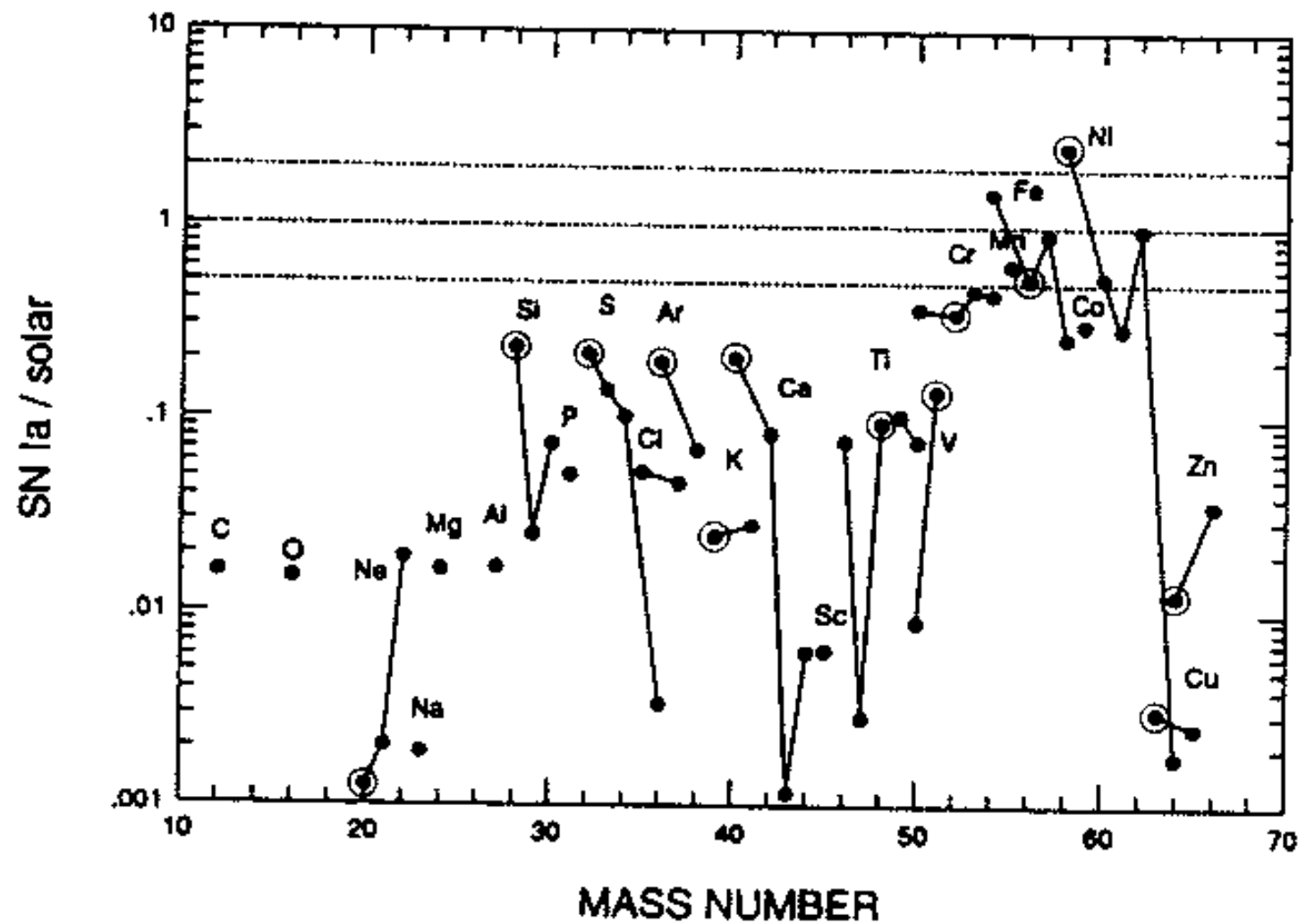


**Fig. 5.25.** Nucleosynthetic outcome (after radioactive decay) of model W7 for Type Ia supernovae (Nomoto, Thielemann & Yokoi 1984, and Thielemann, Nomoto & Yokoi 1986), compared to Solar-System abundances. Dominant isotopes of multi-isotope elements are circled. Adapted from Tsujimoto (1993).